

# Observation of terahertz magnon of Kaplan-Kittel exchange resonance in yttrium-iron garnet by Raman spectroscopy

Wei-Hung Hsu,<sup>1,\*</sup> Ka Shen,<sup>2</sup> Yasuhiro Fujii,<sup>3</sup> Akitoshi Koreeda,<sup>3</sup> and Takuya Satoh<sup>1,4,†</sup>

<sup>1</sup>*Department of Physics, Kyushu University, Fukuoka 819-0395, Japan*

<sup>2</sup>*Center for Advanced Quantum Studies and Department of Physics,  
Beijing Normal University, Beijing 100875, China*

<sup>3</sup>*Department of Physical Sciences, Ritsumeikan University, Kusatsu 525-8577, Japan*

<sup>4</sup>*Department of Physics, Tokyo Institute of Technology, Tokyo 152-8551, Japan*

(Dated: December 22, 2024)

Backscattering Raman spectroscopic investigations were performed on an yttrium-iron garnet single crystal using linearly and circularly polarized light. A THz magnon of the Kaplan-Kittel (KK) exchange resonance was discovered, which had been regarded as unobservable by optical methods. The KK exchange resonance had 7.8 THz frequency at 80 K, and the polarization selection rule led to an antisymmetric Raman tensor of  $A_2$  mode. Besides, assignment of all the Raman-active phonon modes,  $3A_{1g}$ ,  $8E_g$ , and  $14T_{2g}$ , was completed. This study will stimulate further investigation on the coupling of THz magnons and phonons and pave the way toward THz opto-magnonics.

Yttrium-iron garnet ( $\text{Y}_3\text{Fe}_5\text{O}_{12}$ , YIG), which possesses superior properties such as long-lived spin waves with very low damping ( $\alpha \approx 10^{-5}$ ) and a high Curie temperature ( $T_c = 560$  K), has been regarded as an important magnetic material since its discovery over 60 years ago [1–4]. YIG is a ferrimagnetic insulator that is one of the best candidates for applications in spintronics [5], magnonics [6, 7], and spin caloritronics [8]. For developing magnetic devices with ultrafast responses, studies on THz magnon mechanisms are inevitable [9–14]. However, previous studies on YIG mostly focused on applications of acoustic magnons with frequencies in the GHz range [15–19]. Existing studies provide limited information about the properties of THz optical magnons in YIG [4]. Recent investigations on full magnon band structures have been based on several theoretical methods [20–24]. In experimental studies, the THz magnons in YIG have only been identified using inelastic neutron scattering spectroscopy [25–28]. Hence, to understand the behaviors of the THz magnons in YIG in further detail, it is necessary to investigate other optical properties such as the selection rule using Raman spectroscopy.

YIG contains 20 Fe atoms in the primitive bcc unit cell. The magnetic moment is carried by  $\text{Fe}^{3+}$  spins in the 12 tetrahedral d-sites (majority) and 8 octahedral a-sites (minority) with an antiparallel state in the unit cell, forming a two-sublattice ferrimagnet [3]. Among the 20 magnon modes, there are two types of modes with opposite precession directions. Twelve modes belong to the anticlockwise (along the direction of the applied magnetic field) mode, which has a relatively low frequency and inconspicuous temperature-dependent frequency shift. The other eight modes belong to the clockwise mode, which has a relatively higher frequency and significant temperature-dependent frequency shift [20].

On the other hand, in a ferrimagnet with two sublattices, there are two uniform modes at wave number  $k = 0$ , namely, an acoustic mode (Kittel mode) with anticlockwise rotation and an optical mode with clockwise rotation [29–31]. The optical mode is identical to the Kaplan-Kittel (KK) exchange resonance [32] between a-site and d-site Fe sublattices, which has been considered unobservable using optical [infrared (IR) or Raman] methods [29] and has never been observed till date [33, 34].

Therefore, in this study, we investigated the magnetic and crystallographic properties of a single-crystal YIG using polarized-backscattering Raman spectroscopy. Considering the temperature dependence of Raman shift from 80 to 150 K, we clearly identified a THz magnon of the KK exchange resonance. With regard to the crystallographic properties, although the phonon modes of YIG have been studied using Raman spectroscopy for decades, not all the phonon modes have been observed [34–37]. Here, using linearly and circularly polarized light, we completed the phonon-mode assignment of YIG.

The a-site and d-site magnetizations of the Fe sublattices in YIG are defined as  $\mathbf{M}_a$  and  $\mathbf{M}_d$ , respectively. Under an effective magnetic field, the magnetization during precessional motion in response to torques is described by the Landau-Lifshitz-Gilbert (LLG) equation. The LLG equations for  $\mathbf{M}_a$  and  $\mathbf{M}_d$  neglecting damping can be written as follows:

$$\begin{aligned}\frac{d\mathbf{M}_a}{dt} &= -\gamma \mathbf{M}_a \times \mathbf{H}_a, \\ \frac{d\mathbf{M}_d}{dt} &= -\gamma \mathbf{M}_d \times \mathbf{H}_d,\end{aligned}\tag{1}$$

where  $\gamma$  is the gyromagnetic ratio of iron that is invariant in both a- and d-site sublattices. The effective magnetic fields  $\mathbf{H}_a$  and  $\mathbf{H}_d$  acting on  $\mathbf{M}_a$  and  $\mathbf{M}_d$  can be expressed as  $\mathbf{H}_a = -\lambda \mathbf{M}_d$  and  $\mathbf{H}_d = -\lambda \mathbf{M}_a$ , respectively, as shown in Fig. 1(a). The Weiss constant  $\lambda$  is positive. Assuming  $\mathbf{M}_a = (-M_a, m_a^y, m_a^z)$  and  $\mathbf{M}_d = (M_d, m_d^y, m_d^z)$ , the precessional motions with time dependence  $\exp(i\omega t)$  can be derived from Eq. (1). The frequency of the KK exchange

\* jacky81418@gmail.com

† satoh@phys.titech.ac.jp

resonance is obtained as follows [32]:

$$\omega = \lambda\gamma |M_a - M_d|. \quad (2)$$

Here, the effective fields arising from magnetic anisotropy, demagnetization, and magnetic dipoles are omitted because their contributions to the resonance frequency are negligibly small.

Because the magnetizations in the a- and d-site sublattices orientate in opposite directions with strength ratio  $|M_d| : |M_a| = 3 : 2$ , the ferromagnetic  $\mathbf{M} = \mathbf{M}_a + \mathbf{M}_d$  and antiferromagnetic vectors  $\mathbf{L} = \mathbf{M}_d - \mathbf{M}_a$  coexist in YIG [see Fig. 1(b)].  $\mathbf{M}$  and  $\mathbf{L}$  would also exhibit precessional motion under the effective fields  $\mathbf{H}$  and  $\mathbf{h}$  expressed as follows:

$$\begin{aligned} \mathbf{H} &= \mathbf{H}_d + \mathbf{H}_a = -\lambda\mathbf{M}, \\ \mathbf{h} &= \mathbf{H}_d - \mathbf{H}_a = \lambda\mathbf{L}. \end{aligned} \quad (3)$$

The LLG equations for the vectors  $\mathbf{M}$  and  $\mathbf{L}$  are as follows:

$$\begin{aligned} \frac{d\mathbf{M}}{dt} &= -\frac{\gamma}{2} (\mathbf{M} \times \mathbf{H} + \mathbf{L} \times \mathbf{h}), \\ \frac{d\mathbf{L}}{dt} &= -\frac{\gamma}{2} (\mathbf{M} \times \mathbf{h} + \mathbf{L} \times \mathbf{H}). \end{aligned} \quad (4)$$

Assuming  $\mathbf{M} = (M, m_y, m_z)$  and  $\mathbf{L} = (5M, l_y, l_z)$  according to the ratio of  $\mathbf{M}_d$  and  $\mathbf{M}_a$  in YIG, the time-dependent motions of  $\mathbf{M}$  and  $\mathbf{L}$  in the  $y$ - $z$  plane are expressed as follows:

$$\frac{dm_y}{dt} = \frac{dm_z}{dt} = 0, \quad (5)$$

$$\begin{aligned} \frac{dl_y}{dt} &= -\lambda\gamma M (5m_z - l_z), \\ \frac{dl_z}{dt} &= -\lambda\gamma M (l_y - 5m_y). \end{aligned} \quad (6)$$

Equation (5) shows that the ferromagnetic vector  $\mathbf{M}$  is not in precessional motion [see Fig. 1(d)]; this implies that the projecting vectors of the  $y$ - $z$  plane, namely,  $\mathbf{M}_d$  and  $\mathbf{M}_a$ , are not only antiparallel but also equivalent [see Fig. 1(c)]. On the other hand, the antiferromagnetic vector  $\mathbf{L}$  precesses clockwise, and the precessional frequency obtained using Eq. (6) is the same as that obtained using Eq. (2), namely,  $\omega = \lambda\gamma M$ . This frequency is equivalent to  $(12 \cdot S_d - 8 \cdot S_a) |J_{ad}| = 10 |J_{ad}|$ , where  $S_a = S_d = 5/2$ ,  $J_{ad}$  is the exchange constant between the magnetizations at the a- and d-site sublattices [23]. Thus, the KK exchange resonance is identical to the clockwise uniform mode at  $k = 0$  [29, 30] ( $\alpha_1$  mode in Ref. [23]).

In our  $180^\circ$  backscattering Raman spectroscopy system, the exciting light with a power of 40 mW from a diode laser (LD785-SEV300, Thorlabs) with a wavelength of 785 nm was linearly and circularly polarized using polarizers, half-wave plates, and quarter-wave plates. The focused laser spot was  $25 \mu\text{m}$  in diameter and the

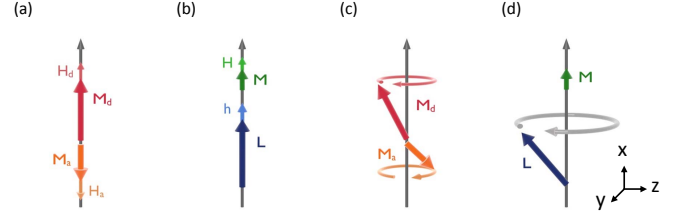


FIG. 1. Schematic of KK exchange resonance mode. (a) Sublattice magnetizations  $\mathbf{M}_a$  and  $\mathbf{M}_d$  under effective magnetic fields  $\mathbf{H}_a$  and  $\mathbf{H}_d$  in the ground state, respectively. (b) Ferromagnetic and antiferromagnetic vectors  $\mathbf{M}$  and  $\mathbf{L}$  under effective magnetic fields  $\mathbf{H}$  and  $\mathbf{h}$  in the ground state, respectively. (c) In KK exchange resonance,  $\mathbf{M}_a$  and  $\mathbf{M}_d$  precess in the clockwise direction. (d)  $\mathbf{L}$  also precesses in the same direction, while  $\mathbf{M}$  is stationary.

frequency resolution of our Raman system was  $1.0 \text{ cm}^{-1}$ . Heating from the focused laser spot of our system affected the Raman spectrum by  $1\text{--}2 \text{ cm}^{-1}$  in red shift. To select the specific polarized light scattered from the sample, a Glan-Taylor prism was set before the monochromator (Acton SpectraPro 2500i, Princeton Instruments). In accordance with the selection of polarization of the incident and scattered light, two linear configurations [parallel ( $\parallel$ ) and crossed ( $\perp$ )] and four circular configurations (RL, LR, RR, and LL) were defined. The helicity of the circularly polarized light was defined as the direction of polarization rotation in the sample plane, irrespective of the propagation direction. Temperature-dependent measurements were performed using liquid nitrogen.

Before we searched for the KK magnetic resonance, we investigated the phonon modes using angle-resolved polarized Raman spectroscopy [38] to distinguish the magnon and phonon modes. An YIG single crystal grown by the floating zone technique was oriented along the  $[111]$  direction and polished to a thickness of  $160 \mu\text{m}$ . YIG belongs to the cubic centrosymmetric space group  $Ia\bar{3}d$  and crystallographic point group  $m\bar{3}m$  [2]. The phonon Raman tensors are described in the Supplemental Material [39] where the bases of the Raman tensors [40] are transformed to  $\hat{\mathbf{x}} \parallel [11\bar{2}]$ ,  $\hat{\mathbf{y}} \parallel [\bar{1}10]$ , and  $\hat{\mathbf{z}} \parallel [111]$ .

For the crystallographic point group  $m\bar{3}m$ , all the three Raman-active phonon modes, namely,  $A_{1g}$ ,  $E_g$ , and  $T_{2g}$ , are not expected to have polarization azimuth dependence on linearly polarized light propagating along the  $z$  direction. On the other hand, we have the Jones vectors  $|H\rangle = (1, 0)$  for horizontal polarization,  $|V\rangle = (0, 1)$  for vertical polarization,  $|R\rangle = (1, -i)/\sqrt{2}$  for right-handed circular polarization, and  $|L\rangle = (1, i)/\sqrt{2}$  for left-handed circular polarization [41]. Therefore, the Raman intensity ratios  $[I_{\parallel} : I_{\perp} : I_{RL} : I_{RR}]$  of  $A_{1g}$ ,  $E_g$ , and  $T_{2g}$  are calculated to be  $[1 : 0 : 0 : 1]$ ,  $[1 : 1 : 2 : 0]$ , and  $[3 : 2 : 4 : 1]$ , respectively [42]. Further,  $I_{LR} = I_{RL}$  and  $I_{LL} = I_{RR}$ . In addition, an in-plane magnetic field of 2.5 kOe was applied using permanent magnets to magnetically saturate our sample. This ensured that Faraday rotation of the incident and scattered light in the sample

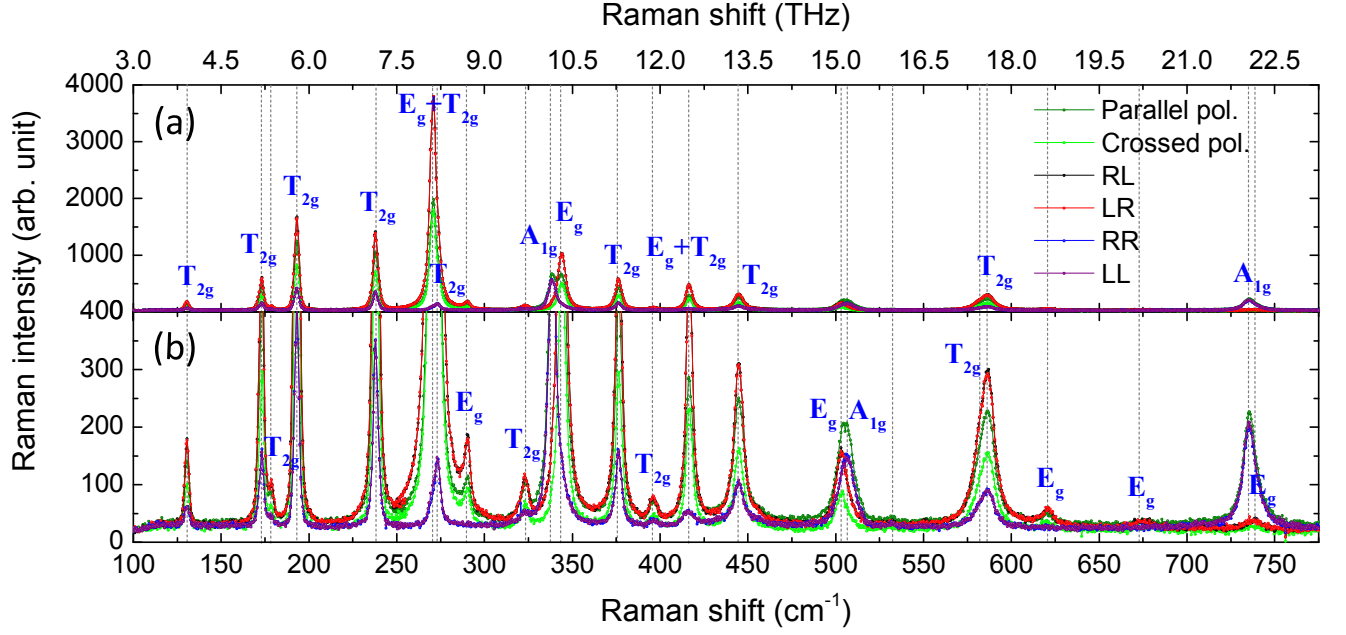


FIG. 2. (a) Full Raman spectra with various polarization configurations at 80 K. For linear polarization, dark and light green spectra represent parallel and crossed configurations, respectively. For circular polarization, black, red, blue, and purple spectra represent RL, LR, RR, and LL configurations, respectively. (b) Magnifications of (a).

did not influence the Raman selection rules.

Figures 2(a) and 2(b) show Raman spectra ranging from  $100 \text{ cm}^{-1}$  to  $775 \text{ cm}^{-1}$  at 80 K and their magnifications, respectively. In previous studies, with only linearly polarized configurations, some ambiguous peaks could not be distinguished [34, 35]. However, in the present study, using both linearly and circularly polarized configurations, all the phonon modes, namely,  $3A_{1g}$ ,  $8E_g$ , and  $14T_{2g}$ , in YIG were successfully assigned and are listed in Table I.

By considering the frequency region of the THz magnon as reported in the latest study [21–24, 26, 27], we focused on spectra in the range from  $210 \text{ cm}^{-1}$  to  $320 \text{ cm}^{-1}$ , as shown in Fig. 3. In the spectra obtained for the RR configuration, we found that a tiny signal significantly shifted from 80 to 150 K, and it blended into the tail of the  $T_{2g}$  phonon signal above 150 K. An almost identical signal was also observed for the LL configuration (not shown). Because of the significant temperature dependence of the frequency shift, the tiny signal was assigned to the THz magnon. The wave number  $k$  of the detected magnon in the  $180^\circ$  backscattering geometry was  $4\pi n/\lambda$  ( $n$ : refractive index,  $\lambda$ : incident light wavelength). Therefore,  $a_0 k \approx 0.05 \text{ rad} \ll 1$  (lattice constant of YIG,  $a_0 = 1.24 \text{ nm}$  [2]), meaning that the THz magnon of the KK exchange resonance with  $\mathbf{k} \approx 0$  was excited at 7.8 THz, the frequency corresponding to  $260 \text{ cm}^{-1}$  at 80 K.

Furthermore, the temperature-dependent frequency shifts of the THz magnon in our RR and LL spectra were identified and compared to the results obtained from

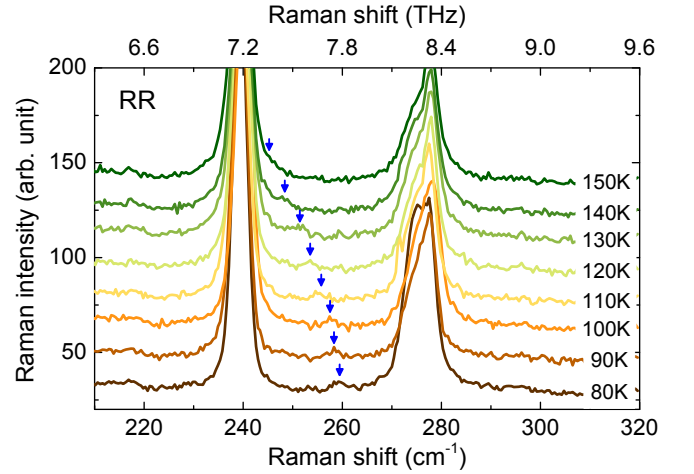


FIG. 3. Raman spectra of YIG (111) in the range from  $210 \text{ cm}^{-1}$  to  $320 \text{ cm}^{-1}$  with RR polarized configuration from 80 to 150 K. The tiny signal indicated by blue arrows exhibits significant temperature-dependent frequency shifts unlike other phonon signals.

neutron scattering measurements [25, 28] and simulations [23, 24], as shown in Fig. 4 (a). Our results show the same tendency as reported in other studies. However, there is a frequency deviation between our results and the others. The exchange constant  $J_{\text{ad}}$  was determined in previous studies based on the results of magnetization, specific heat measurement, inelastic neutron scattering, or first-principles calculations. However, we

consider that Raman spectroscopy provides more precise frequency resolution than other techniques. By extrapolating the magnon frequency of 7.8 THz at 80 K down to 4 K based on the temperature dependence of magnetization [43], we obtained a frequency of 8.0 THz at 4 K. This yields  $J_{\text{ad}} = -38$  K according to  $10|J_{\text{ad}}| = 8.0$  THz. Furthermore, the in-plane magnetic field of 2.5 kOe did not affect the magnon frequency within the experimental resolution.

Moreover, we focused on the same frequency range and repeated the Raman measurements with all linearly and circularly polarized configurations at 80 K; the results are shown in Fig. 4(b). The Raman intensity ratio of the KK mode was  $[I_{\parallel} : I_{\perp} : I_{\text{RL}} : I_{\text{RR}}] = [0 : 1 : 0 : 1]$ , indicating that the magnon Raman tensor can be expressed in the antisymmetric form as

$$R = \begin{pmatrix} 0 & iK \\ -iK & 0 \end{pmatrix}.$$

This antisymmetric form of the KK mode corresponds to linear (first order) magnetic excitation, where  $K$  is proportional to  $m_z$  [44–48]. The similarity of the KK mode to the one in the GHz acoustic magnon (Kittel mode) excited through light scattering [17–19] indicates that the

TABLE I. Assignment of phonon signals in YIG (111) Raman spectra at 80 K. All shifts are in units of  $\text{cm}^{-1}$ .

[34]	Mode	[35]	Mode	This study	Mode
130	$T_{2g}$	131	$T_{2g}$	132	$T_{2g}$
175	$T_{2g}$	174	$T_{2g}$	174	$T_{2g}$
				178	$T_{2g}$
193	$T_{2g}$	194	$T_{2g}$	194	$T_{2g}$
237	$T_{2g}$	238	$T_{2g}$	239	$T_{2g}$
274	$E_g$	274	$E_g + T_{2g}$	272	$E_g + T_{2g}$
				274	$T_{2g}$
				290	$E_g$
315	$E_g$	319	$E_g$	323	$T_{2g}$
		324	$T_{2g}$	340	$A_{1g}$
347	$E_g + A_{1g}$	346	$E_g$	345	$E_g$
380	$T_{2g}$	378	$T_{2g}$	377	$T_{2g}$
				396	$T_{2g}$
		416	$E_g$	416	$E_g + T_{2g}$
420	$E_g + T_{2g}$	419	$T_{2g}$		
449	$T_{2g} + A_{1g}$	445	$T_{2g}$	446	$T_{2g}$
		456	$E_g$		
507	$A_{1g}$	504	$A_{1g}$	505	$E_g$
				507	$A_{1g}$
593	$T_{2g}$	592	$T_{2g}$	581	$T_{2g}$
		624	$E_g$	587	$T_{2g}$
				620	$E_g$
				675	$E_g$
698	$A_{1g} + E_g$	685	$E_g + T_{2g}$		
		692	$E_g + T_{2g}$		
		704	$A_{1g}$		
		711	$T_{2g}$		
		736	$A_{1g}$ or $E_g + T_{2g}$	737	$A_{1g}$
740	$A_{1g}$			739	$E_g$

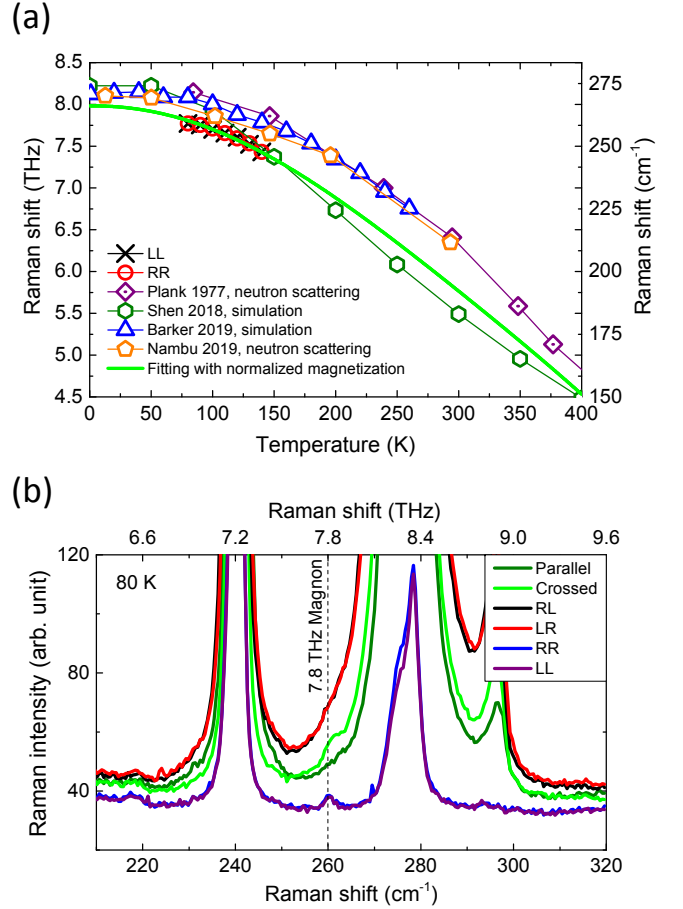


FIG. 4. (a) Temperature-dependent frequency shift of KK mode. The black line with crosses and red line with circles denote the KK mode observed in our Raman spectra with RR and LL configurations, respectively. The purple line with squares [25] and orange line with pentagons [28] represent the experimental data for neutron scattering. The blue line with triangles [24] and green line with hexagons [23] indicate the simulation results obtained using different models. The KK mode is fitted with normalized magnetization (yellowish green) [43]. (b) The selection rule for KK mode of YIG observed with crossed, RR, and LL polarized configurations at 7.8 THz and 80 K.

KK and Kittel modes have the same symmetry. In the KK mode, all the atomic spins from the same sublattice simultaneously rotate with their spins always parallel and having the same precession amplitude, similar to the Kittel mode in the ferromagnetic subsystem. The other sublattice behaves in the same way. Therefore, the direction of precessional motion of each sublattice is reversed under mirror operations ( $\sigma_v$  or  $\sigma_d$ ), which corresponds to the  $A_2$  mode [49].

Symmetric contributions owing to quadratic (second order) excitation [46, 48, 50–52] were not observed in the present study, probably because the linear magneto-optical (Faraday) effect dominated the quadratic magneto-optical (Cotton-Mouton) effect at a

wavelength of 785 nm [53].

In addition, unlike the acoustic magnon, the ferromagnetic vector  $\mathbf{M}$  of the KK mode does not precess, as shown in Fig. 1(d). Nevertheless, the KK mode was observed as a linear magnetic excitation, which usually results from the precession of  $\mathbf{M}$ . This contradiction can be explained as follows. The absorption coefficient of YIG at 785 nm is 50–100 cm<sup>-1</sup> [54–56]. This is attributed to off-resonant transition with the nearest resonances at 900 nm ( ${}^6A_{1g} \rightarrow {}^4T_{1g}$ ) and 700 nm ( ${}^6A_{1g} \rightarrow {}^4T_{2g}$ ) in octahedral Fe<sup>3+</sup> ions [55]. The Faraday rotation of 600–800°/cm at 785 nm [53, 57–60] dominantly originates from optical transitions in octahedral Fe<sup>3+</sup> ions [60–63]. Therefore, the Faraday rotation is more sensitive to  $\mathbf{M}_a$  rather than  $\mathbf{M}_d$ . The KK mode resulted from the precessional motion of  $\mathbf{M}_a$  [64].

The KK exchange resonance between iron and rare-earth sublattices is identified in rare-earth iron garnets through IR [65–67] and pump-probe [68, 69] spectroscopy. However, in YIG, because the ferromagnetic vector  $\mathbf{M}$  of the KK mode does not precess owing to the equality of  $\gamma$  for  $\mathbf{M}_a$  and  $\mathbf{M}_d$ , this mode cannot be observed by IR spectroscopy as well as magnetic resonance spectroscopy.

In summary, all the phonon modes, namely,  $3A_{1g}$ ,  $8E_g$ , and  $14T_{2g}$ , in YIG were successfully identified

and assigned using linearly and circularly polarized light through Raman spectroscopy. A THz magnon of the KK exchange resonance in YIG was discovered in Raman spectra at temperatures from 80 to 150 K, and the exchange constant was  $J_{ad} = -38$  K. The selection rule of magneto-optical coupling in YIG was experimentally confirmed, which suggested an antisymmetric magnon Raman tensor ( $A_2$ ) corresponding to the linear magneto-optical effect. This study will stimulate further investigation on the coupling of THz magnons and phonons for applications involving spin caloritronics and pave the way toward THz opto-magnonics.

## ACKNOWLEDGMENTS

We would like to thank J. Barker and G. E. W. Bauer for valuable discussions and a critical proofreading of the manuscript. We also thank P. Maldonado and P. M. Oppeneer for sharing with us their data on phonon dispersion calculations. This study was supported by the Japan Society for the Promotion of Science (JSPS) KAKENHI (Grants No. JP15H05454, No. JP17K18765, No. JP19H01828, No. JP19H05618, No. JP19K21854, and No. JP26103004), JSPS Core-to-Core Program (A. Advanced Research Networks).

- 
- [1] F. Bertaut and F. Forrat, *Compt. Rend.* **242**, 382 (1956).
  - [2] S. Geller and M. A. Gilleo, *J. Phys. Chem. Solids* **3**, 30 (1957).
  - [3] M. A. Gilleo, in *Handbook of Magnetic Materials*, edited by E. P. Wohlfarth, Vol. 2 (North Holland, 1986).
  - [4] V. Cherepanov, I. Kolokolov, and V. L'vov, *Phys. Rep.* **229**, 81 (1993).
  - [5] A. V. Chumak, V. I. Vasyuchka, A. A. Serga, and B. Hillebrands, *Nat. Phys.* **11**, 453 (2015).
  - [6] V. V. Kruglyak, S. O. Demokritov, and D. Grundler, *J. Phys. D* **43**, 264001 (2010).
  - [7] Y. Tabuchi, S. Ishino, T. Ishikawa, R. Yamazaki, K. Usami, and Y. Nakamura, *Phys. Rev. Lett.* **113**, 083603 (2014).
  - [8] G. E. W. Bauer, E. Saitoh, and B. J. van Wees, *Nat. Mater.* **11**, 391 (2012).
  - [9] T. Satoh, S.-J. Cho, R. Iida, T. Shimura, K. Kuroda, H. Ueda, Y. Ueda, B. A. Ivanov, F. Nori, and M. Fiebig, *Phys. Rev. Lett.* **105**, 077402 (2010).
  - [10] B. A. Ivanov, *Low Temp. Phys.* **40**, 91 (2014).
  - [11] D. Bossini and Th. Rasing, *Phys. Scr.* **92**, 024002 (2017).
  - [12] V. Baltz, A. Manchon, M. Tsoi, T. Moriyama, T. Ono, and Y. Tserkovnyak, *Rev. Mod. Phys.* **90**, 015005 (2018).
  - [13] P. Němec, M. Fiebig, T. Kampfrath, and A. V. Kimel, *Nat. Phys.* **14**, 229 (2018).
  - [14] A. V. Kimel, A. M. Kalashnikova, A. Pogrebna, and A. K. Zvezdin, *Phys. Rep.* **852**, 1 (2020).
  - [15] J. F. Dillon, *Phys. Rev.* **105**, 759 (1957).
  - [16] R. C. LeCraw, E. G. Spencer, and C. S. Porter, *Phys. Rev.* **110**, 1311 (1958).
  - [17] B. A. Auld and D. A. Wilson, *J. Appl. Phys.* **38**, 3331 (1967).
  - [18] H. L. Hu and F. R. Morgenthaler, *Appl. Phys. Lett.* **18**, 307 (1971).
  - [19] J. R. Sandercock and W. Wettling, *Solid State Commun.* **13**, 1729 (1973).
  - [20] J. Barker and G. E. W. Bauer, *Phys. Rev. Lett.* **117**, 217201 (2016).
  - [21] L.-S. Xie, G.-X. Jin, L. He, G. E. W. Bauer, J. Barker, and K. Xia, *Phys. Rev. B* **95**, 014423 (2017).
  - [22] Y. Liu, L.-S. Xie, Z. Yuan, and K. Xia, *Phys. Rev. B* **96**, 174416 (2017).
  - [23] K. Shen, *New J. Phys.* **20**, 043025 (2018).
  - [24] J. Barker and G. E. W. Bauer, *Phys. Rev. B* **100**, 140401 (2019).
  - [25] J. S. Plant, *J. Phys. C* **10**, 4805 (1977).
  - [26] A. J. Princep, R. A. Ewings, S. Ward, S. Tóth, C. Dubs, D. Prabhakaran, and A. T. Boothroyd, *npj Quantum Mater.* **2**, 63 (2017).
  - [27] S. Shamoto, T. U. Ito, H. Onishi, H. Yamauchi, Y. Inamura, M. Matsuura, M. Akatsu, K. Kodama, A. Nakao, T. Moyoshi, K. Munakata, T. Ohhara, M. Nakamura, S. Ohira-Kawamura, Y. Nemoto, and K. Shibata, *Phys. Rev. B* **97**, 054429 (2018).
  - [28] Y. Nambu, J. Barker, Y. Okino, T. Kikkawa, Y. Shiomi, M. Enderle, T. Weber, B. Winn, M. Graves-Brook, J. M. Tranquada, T. Ziman, M. Fujita, G. E. W. Bauer, E. Saitoh, and K. Kakurai, *arXiv:1911.11968* (2019).
  - [29] R. L. Douglass, *Phys. Rev.* **120**, 1612 (1960).
  - [30] A. B. Harris, *Phys. Rev.* **132**, 2398 (1963).
  - [31] W. F. Brinkman and R. J. Elliott, *P. Roy. Soc. A-Math. Phys.* **294**, 343 (1966).

- [32] J. Kaplan and C. Kittel, J. Chem. Phys. **21**, 760 (1953).
- [33] K. M. Häussler, H. J. Falge, and J. Brandmüller, J. Raman Spectrosc. **10**, 185 (1981).
- [34] P. Grunberg, J. A. Koningstein, and L. G. Van Uitert, J. Opt. Soc. Am. **61**, 1613 (1971).
- [35] J.-J. Song, P. B. Klein, R. L. Wadsack, M. Selders, S. Mroczkowski, and R. K. Chang, J. Opt. Soc. Am. **63**, 1135 (1973).
- [36] E. J. J. Mallmann, A. S. B. Sombra, J. C. Goes, and P. B. A. Fechine, Solid State Phenom. **202**, 65 (2013).
- [37] J.-M. Costantini, S. Miro, F. Beuneu, and M. Toulemonde, J. Phys. Condens. Matter **27**, 496001 (2015).
- [38] Y. Fujii, M. Noju, T. Shimizu, H. Taniguchi, M. Itoh, and I. Nishio, Ferroelectrics **462**, 8 (2014).
- [39] See Supplemental Material for the phonon Raman tensors.
- [40] W. Hayes and R. Loudon, *Scattering of Light by Crystals* (Wiley, New York, 1978).
- [41] A. Yariv and P. Yeh, *Photonics: Optical Electronics in Modern Communications*, 6th ed. (Oxford University Press, USA, 2006).
- [42] P. Khan, M. Kanamaru, W.-H. Hsu, M. Kichise, Y. Fujii, A. Koreeda, and T. Satoh, J. Phys. Condens. Matter **31**, 275402 (2019).
- [43] E. E. Anderson, Phys. Rev. **134**, A1581 (1964).
- [44] P. A. Fleury and R. Loudon, Phys. Rev. **166**, 514 (1968).
- [45] H. Le Gall and J. P. Jamet, Phys. Status Solidi B **46**, 467 (1971).
- [46] W. Wettling, M. G. Cottam, and J. R. Sandercock, J. Phys. C **8**, 211 (1975).
- [47] A. S. Borovik-Romanov and N. M. Kreines, Phys. Rep. **81**, 351 (1982).
- [48] R. Hisatomi, A. Noguchi, R. Yamazaki, Y. Nakata, A. Gloppe, Y. Nakamura, and K. Usami, Phys. Rev. Lett. **123**, 207401 (2019).
- [49] A. P. Cracknell, J. Phys. C: Solid State Phys. **2**, 500 (1969).
- [50] J. F. Dillon, J. P. Remeika, and C. R. Staton, J. Appl. Phys. **41**, 4613 (1970).
- [51] R. V. Pisarev, I. G. Siniĭ, N. N. Kolpakova, and Y. M. Yakovlev, Sov. Phys. JETP **33**, 1175 (1971).
- [52] J. Ferré and G. A. Gehring, Rep. Prog. Phys. **47**, 513 (1984).
- [53] W. Wettling, Appl. Phys. **6**, 367 (1975).
- [54] J. F. Dillon, J. Phys. Radium **20**, 374 (1959).
- [55] D. L. Wood and J. P. Remeika, J. Appl. Phys. **38**, 1038 (1967).
- [56] G. B. Scott, D. E. Lacklison, and J. L. Page, Phys. Rev. B **10**, 971 (1974).
- [57] A. M. Clogston, J. Appl. Phys. **31**, S198 (1960).
- [58] H. Takeuchi, S. Ito, I. Mikami, and S. Taniguchi, J. Appl. Phys. **44**, 4789 (1973).
- [59] G. B. Scott, D. E. Lacklison, H. I. Ralph, and J. L. Page, Phys. Rev. B **12**, 2562 (1975).
- [60] P. Hansen and K. Witter, Phys. Rev. B **27**, 1498 (1983).
- [61] R. V. Pisarev, J. Schoenes, and P. Wachter, Solid State Commun. **23**, 657 (1977).
- [62] M. Deb, E. Popova, A. Fouchet, and N. Keller, J. Phys. D **45**, 455001 (2012).
- [63] S. F. Maehrlein, I. Radu, P. Maldonado, A. Paarmann, M. Gensch, A. M. Kalashnikova, R. V. Pisarev, M. Wolf, P. M. Oppeneer, J. Barker, and T. Kampfrath, Sci. Adv. **4**, eaar5164 (2018).
- [64] A. H. M. Reid, A. V. Kimel, A. Kirilyuk, J. F. Gregg, and Th. Rasing, Phys. Rev. Lett. **105**, 107402 (2010).
- [65] A. J. Sievers and M. Tinkham, Phys. Rev. **129**, 1995 (1963).
- [66] J. Yamamoto, B. T. Smith, and E. E. Bell, J. Opt. Soc. Am. **64**, 880 (1974).
- [67] T. D. Kang, E. Standard, K. H. Ahn, A. A. Sirenko, G. L. Carr, S. Park, Y. J. Choi, M. Ramazanoglu, V. Kiryukhin, and S.-W. Cheong, Phys. Rev. B **82**, 014414 (2010).
- [68] S. Parchenko, A. Stupakiewicz, I. Yoshimine, T. Satoh, and A. Maziewski, Appl. Phys. Lett. **103**, 172402 (2013).
- [69] S. Parchenko, T. Satoh, I. Yoshimine, F. Stobiecki, A. Maziewski, and A. Stupakiewicz, Appl. Phys. Lett. **108**, 032404 (2016).